Lagrangian velocity and acceleration measurements in plume-rich regions of turbulent Rayleigh-Bénard convection

Xiao-Ming Li,[1,2,3] Shi-Di Huang ◉,[1,3] Rui Ni,[2,*] and Ke-Qing Xia ◉[1,2,3,†]

[1]*Center for Complex Flows and Soft Matter Research and Department of Mechanics and Aerospace Engineering, Southern University of Science and Technology, Shenzhen 518055, China*
[2]*Department of Physics, Chinese University of Hong Kong, Shatin, Hong Kong, China*
[3]*Guangdong Provincial Key Laboratory of Turbulence Research and Applications, Department of Mechanics and Aerospace Engineering, Southern University of Science and Technology, Shenzhen 518055, China*

We report an experimental study of Lagrangian velocity and acceleration in turbulent Rayleigh-Bénard convection using particle tracking velocimetry, with the Rayleigh number Ra spanning from 5.4×10^8 to 1.3×10^{10}. The measurements were made in two representative regions of a cylindrical convection cell with aspect ratio unity, where an abundant amount of thermal plumes are passing through constantly. The results are compared with those obtained in the cell's central region, where plumes are passing through much less frequently. It is found that the probability density functions (pdf's) of the three velocity components almost collapse with each other and follow Gaussian distribution for all the regions in the high Ra range, but they behave differently and deviate from the Gaussian function for lower Ra numbers. For the acceleration, the pdf's in all the regions exhibit a stretched exponential form, but for lower Ra cases the amount of stretching is much more pronounced in the plume-abundant regions as compared to that in the cell center. This difference is more evident in terms of acceleration variance: for Ra $\lesssim 4.3 \times 10^9$, the acceleration variances in the plume-abundant regions are larger than those in the central region and show a different Ra-dependent power law. As Ra number increases, the acceleration variances obtained in different regions gradually merge into a single master curve that follows the Heisenberg-Yaglom prediction for homogeneous and isotropic turbulence. A consistent transitional behavior is also observed in the kinetic energy dissipation rate. Through a detailed examination of the possible balance relations between acceleration and other small-scale properties, our results show that the acceleration in the plume-abundant regions is balanced with a combination of thermal and kinetic energy dissipation rates, which suggests that the turbulent flow in these regions is governed by a mixed dynamics with contributions from both thermal plumes and turbulent background fluctuations. This picture is supported by a modified Heisenberg-Yaglom relation and also by the scaling behaviors of the Eulerian structure functions in the inertial range. The observed transitional behaviors can be understood as a result of the evolution in the circulation path of the large-scale flow, which changes from an ellipse to a more squarish shape with increasing Ra.

———————

*Present address: Department of Mechanical Engineering, Johns Hopkins University, Baltimore, Maryland 21218, USA.
†Corresponding author: xiakq@sustech.edu.cn

I. INTRODUCTION

Turbulent convection occurs widely in nature and in industrial processes, such as circulations in oceans and atmosphere, cooling of electronic devices, and ventilation of buildings. Turbulent Rayleigh-Bénard (RB) convection, a fluid layer heated from below and cooled from above, has been a paradigm for studying the general mechanism of convection phenomena [1–4]. A prominent feature of turbulent RB convection is the ubiquity of thermal plumes [see Fig. 1(a)]. These coherent structures are generated from the thermal boundary layers and they are found to play important roles in various dynamic processes of the turbulent convective flow.

Through simultaneous measurements of local velocity and temperature, it is revealed that thermal plumes are dominant heat carriers in turbulent convection [5,6]. This was later confirmed by measurements of heat transport using a mobile temperature sensor [7] and the local heat flux data obtained from numerical simulations [8]. Recent studies even demonstrated that thermal plumes can be manipulated to control global heat transfer efficiency [9–11]. Such manipulation is essentially based on modifying the statistical and geometrical properties of thermal plumes, which have been also investigated in a number of studies [12,13]. It is shown that thermal plumes are "cliff-ramp" structures and their statistical properties exhibit log-normal distribution [14,15]. Through direct visualization of thermal plumes, it is further found that their geometrical and other physical properties, such as area, length, and "heat content," also exhibit log-normal distributions [16–18]. In order to examine plumes more quantitatively, several extraction schemes have been developed, using certain criteria that are combinations of plume-related quantities, such as temperature, velocity, vorticity, and thermal dissipation rate [19–21]. These studies enrich our understanding of thermal plumes and their role in heat transport of turbulent convection.

Thermal plumes also play a primary role in the formation and the dynamics of the large-scale circulation in the system, known as the "wind of turbulence" [22–26]. Therefore, it is crucial to understand how thermal plumes supply energy to the turbulent wind [2,27–30]. As thermal plumes have temperature contrast with the background fluid, it is natural to expect that they provide energy to the turbulent wind via their buoyancy. This is somewhat supported by the turbulent energy production $P = -\langle u_i u_j \rangle \partial U_i / \partial x_j$ measured by the particle image velocimetry technique [31–33]. The overall positive value of turbulent energy production implies that the turbulent wind in RB convection is not driven by Reynolds stresses as in some other types of turbulent flows [34], which leaves the buoyancy force associated with thermal plumes as the most plausible driving source. In fact, by assuming a balance between buoyancy and drag forces, several low-dimensional models successfully reproduced some dominating features of the wind [35,36]. However, a later study found that the turbulent energy production contributed by buoyancy flux is much smaller than that due to shear force [37]. This is in line with an experimental study of a dye concentration field in turbulent RB convection [38]. It is found there that all the geometric properties of this passive scalar measured in a plume-abundant region, which are presumably buoyancy-dominant, manifest no effect of buoyancy force. These studies are mostly based on some inferences or estimations, so direct measurements are needed.

One direct method to examine how thermal plumes supply energy to the turbulent wind is to study the small-scale phenomenology [2,39]. In particular, a commonly examined quantity is the nth-order Eulerian velocity structure function (SF) $S_n(r) = \langle |\Delta u(r)|^n \rangle \sim r^{\zeta_n}$, where $\Delta u(r)$ is the Eulerian velocity increment with a separation scale r. Based on simple dimensional analysis, the scaling exponent ζ_n in the inertial range for nonbuoyant flows is expected to obey the Kolmogorov theory as $\zeta_n = n/3$ when intermittency is neglected [40], and if buoyancy force becomes dominant, ζ_n is replaced by the Bolgiano-Obukhov (BO) scaling, i.e., $\zeta_n = 3n/5$ [41,42]. Therefore, by evaluating the power-law scaling of the SF, the role of buoyancy in the plume-abundant regions could be revealed. In the past decades, numerous efforts have been devoted to the search for the so-called BO scaling in turbulent RB convection, but a conclusive evidence for its existence is still missing [43–50].
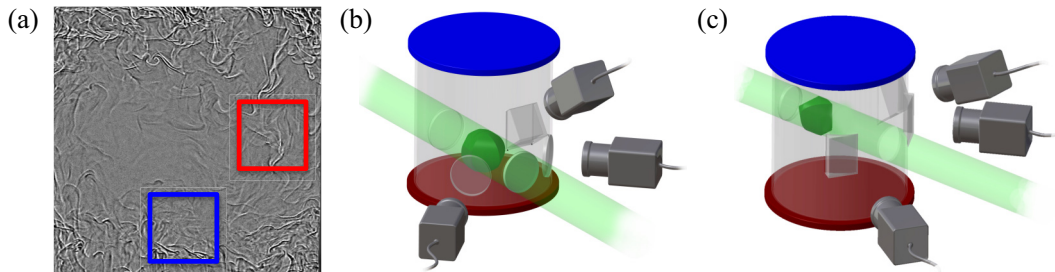
FIG. 1. (a) A typical shadowgraph image of turbulent RB convection measured at Ra $\simeq 1 \times 10^{10}$ and Pr = 4.3. The squared boxes indicate the two measurement regions with abundant plumes passing through. (b) and (c): Sketches of the experimental setups for particle tracking measurements in the bottom and sidewall regions, respectively. The light green indicates the laser beam and the dark green indicates the measurement volume.

On the other hand, to investigate the driving dynamics, one can take the Lagrangian approach rather than the Eulerian one and examine the Boussinesq equations directly,

$$\frac{\partial \mathbf{u}}{\partial t} + (\mathbf{u} \cdot \nabla)\mathbf{u} = -\frac{\nabla \mathbf{P}}{\rho} + \nu \nabla^2 \mathbf{u} + \alpha g \delta T \hat{z}, \tag{1}$$

where $\mathbf{u}$ and $\mathbf{P}$ are the velocity and pressure fields, respectively, and $\alpha g \delta T \hat{z}$ is the buoyancy term under the Boussinesq approximation. Note that the substantive derivative term in the equations is just the acceleration of a fluid parcel, a quantity that has become reliably measurable with the rapid development of Lagrangian particle tracking technique [51–59]. Therefore, one may also examine the acceleration properties to address the issue raised above: Do thermal plumes directly drive the turbulent wind in RB convection via buoyancy force? Of course, this approach is difficult for experiments, as directly measuring the pressure term in the equations is technically challenging. However, we can reasonably resort to some analytical relations to examine whether, and if so how, the acceleration could be balanced with different forces. Indeed, in a previous study, we have demonstrated that the acceleration variance in the center region of turbulent RB convection, where plumes are rarely passing by, is balanced by kinetic energy dissipation rate directly [56]. This indicates that the turbulent flow in this region is governed by the Heisenberg-Yaglom relation that holds for homogeneous and isotropic turbulence with the pressure gradient being dominant [60,61].

In the present paper, we will use similar approaches to investigate the Lagrangian properties in the plume-abundant regions. Our results show that the acceleration in these regions is not balanced with local buoyancy force but a combination of thermal and kinetic energy dissipation rates, which suggests that the corresponding turbulent flow is governed by a mixed dynamics with contributions from both thermal plumes and turbulent background fluctuations. This picture is supported by a modified Heisenberg-Yaglom relation and also the scaling behaviors of the Eulerian structure functions in the inertial range.

II. EXPERIMENTAL SETUP AND MEASUREMENT TECHNIQUES

The experiments were carried out in a cylindrical convection cell with height H and diameter D both being 19.2 cm, so the aspect ratio is unity. The sidewall was made of transparent Plexiglas with designed flat windows placed at suitable positions for particle tracking measurements. The heating power was supplied to the bottom copper plate with a resistive film heater and the temperature of the top copper plate was regulated by a circulator, so that the temperature difference ΔT across the fluid layer can be adjusted precisely. The Rayleigh number Ra = $\alpha g \Delta T H^3/\nu\kappa$ was varied from 5.4×10^8 to 1.3×10^{10}, where g is the gravitational acceleration; α, ν, and κ are the thermal expansion coefficient, the kinematic viscosity, and the thermal diffusivity of the working fluid (deionized water here), respectively. To achieve this Ra number range, the Prandtl number Pr = ν/κ was changed a

little from 6.1 to 4.3, which would not affect the main conclusion of the present study with a focus on the Ra dependence [56].

The measurements were made in two representative plume-abundant regions as indicated in Fig. 1(a), with their edges being $\sim$1.5 cm away from the bottom plate and the sidewall of the convection cell, respectively. For the sake of easy presentation, they are denoted as bottom and sidewall regions, respectively. Note that for the present Ra and Pr ranges, the thicknesses of the viscous and thermal boundary layers are ranging from $0.46 \sim 0.78$ cm [62] and $0.04 \sim 0.15$ cm [63], respectively. Therefore, the measurement regions are well outside the boundary layers for all the cases in the present study, and the measured Lagrangian properties are not affected by the boundary layer dynamics. Moreover, in order to eliminate the influence of the complex three-dimensional flow dynamics [1,57], we tilted the convection cell by a small angle to lock the turbulent wind in a fixed azimuthal plane.

The Lagrangian particle tracking system mainly consists of three high speed cameras with a resolution of 1024×1024 pixels^2 and a pulsed Nd:YLF laser with a wavelength of 527 nm. The cameras were placed in three distinct angles and their arrangements are shown in Figs. 1(b) and 1(c). The measurement volumes for both the bottom and sidewall regions were about $(5 \text{ cm})^3$, so that the spatial resolution is at least one order of magnitude smaller than the Kolmogorov length scale $\eta = (\nu^3/\langle\epsilon_u\rangle)^{1/4}$ in the present study (around $0.5 \sim 2.0$ mm), where $\langle\epsilon_u\rangle$ is the kinetic energy dissipation rate obtained from the second-order Eulerian SFs (shown below). The Stokes number for the polyamid particles used (diameter = 50 μm, density = 1.05 g/cm^3) ranges from 10^{-4} to 10^{-3}. Thus, the particles can be safely considered as tracers. Depending on the Ra number for a particular run, the camera frame rate for data acquisition varied from 50 Hz to 100 Hz, which is sufficient to resolve the Kolmogorov timescale $\tau_\eta = (\nu/\langle\epsilon_u\rangle)^{1/2}$ (around $0.5 \sim 3.0$ seconds). Typically, a total measurement time of $\sim$40 minutes was made for each Ra, corresponding to at least several tens of the turnover time of the turbulent wind [64]. This allowed us to obtain at least 10^7 valid events for each Ra, so the results should be statistically converged in the present study.

Before making the measurements, a calibration process is required to build up a transforming relation between the positions in the acquired image and in real space. To be specific, a staircase-shaped target with 99 calibration dots manufactured on its surface was first put into the measurement regions of the convection cell. Then the target was illuminated by a homemade LED array and viewed by three cameras simultaneously. Because the position information of the calibration dots in real space is given by the manufactured drawing, so we can use this information and the acquired image of calibration dots to obtain the coordinates and orientations of the three cameras through an optimization program. These camera parameters determine how we reconstruct the positions of tracer particles from the acquired image to the real space, based on which we further obtain their trajectories. The velocity and acceleration are then calculated by applying a differentiating-filtering Gaussian kernel to the trajectories of tracer particles [52,53]. For other details about the particle tracking method, please refer to our previous work [56]. The data of that study obtained in the central region of the convection cell (denoted as center region) are also used here for comparison.

It is worth pointing out that the temperature fluctuations in the convective flow can cause fluctuations in the optical index of the fluid, which would have an effect on the velocity and acceleration measurements. To evaluate this effect quantitatively, we developed a method by tracking the static dots on the calibration target as "particles." In the case without temperature fluctuations, the detected positions of the calibration dots in the acquired images should be stationary; i.e., their "velocity" and "acceleration" should be zero. However, because of the fluctuations in temperature (and thus optical index), the detected positions of these dots also fluctuate with time. With the virtual "trajectories" of the detected dots, we can calculate the corresponding "velocity" and "acceleration." These results provide a quantitative evaluation of the effect of optical index variations on the velocity and acceleration measurements. In our previous study, we have used this method to demonstrate that this effect is negligible in the central region of the convection cell [56]. For the regions with an abundant amount of thermal plumes, we made a similar evaluation. Because the effect is presumably stronger for larger temperature fluctuations (directly related to the global temperature difference
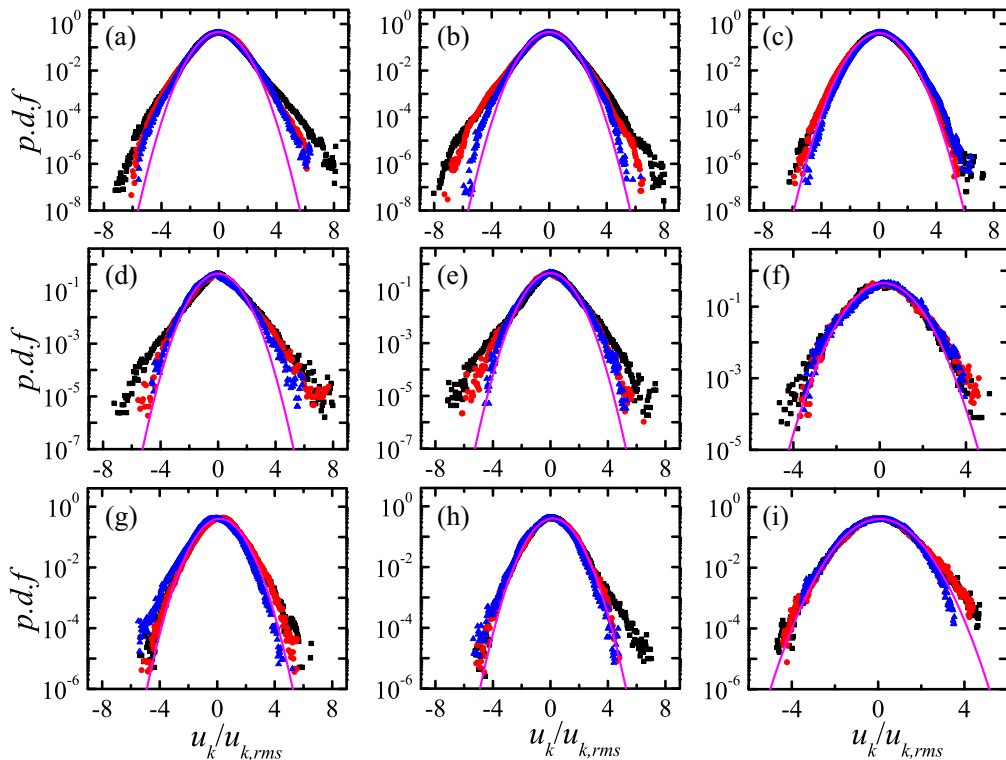
FIG. 2. The probability density functions (pdf's) of the three normalized velocity components measured in different regions and at three representative Ra numbers, where $k = x, y$, and z. From top to bottom: Center region [(a), (b), (c)], sidewall region [(d), (e), (f)], and bottom region [(g), (h), (i)]. Left panel: Ra $\simeq 6 \times 10^8$; middle panel: Ra $\simeq 1.3 \times 10^9$; right panel: Ra $\simeq 1 \times 10^{10}$. For all the pdf's, red circle, blue triangle, and black square represent the x, y, and z components, respectively.

ΔT), we tested the case for $\Delta T = 31.6\,°\text{C}$, which is the highest ΔT for Pr $= 6.1$ explored in the present study. It is found that the maximum difference between the detected and true positions of the calibration dots is smaller than 0.05 mm, corresponding to one pixel in the present experiment. The so obtained maximum root-mean-square (rms) velocity and acceleration are 0.25 mm/s and 0.14 mm/s^2, respectively. These values are much smaller than the typical values for real tracer particles (3.75 mm/s for velocity and 1.87 mm/s^2 for acceleration) obtained at the same ΔT. Therefore, we conclude that the effect of optical index variations on the velocity and acceleration measurements can be safely ignored in the present study.

III. RESULTS AND DISCUSSION

A. Velocity statistics

We first compare the Lagrangian velocity statistics measured in different regions. Figure 2 shows the probability density functions (pdf's) of the three velocity components normalized by their own rms values at three representative Ra numbers. It is found that, for the highest Ra cases, the three velocity components nearly fall on top of each other, and their shapes can be described by a Gaussian function approximately, regardless of the measurement regions. However, when it goes to smaller Ra cases, while the behavior in the bottom region is almost qualitatively the same, those in the center and sidewall regions become apparently different: the three components do not collapse well anymore, and their shapes are found to be non-Gaussian and asymmetric. These results suggest
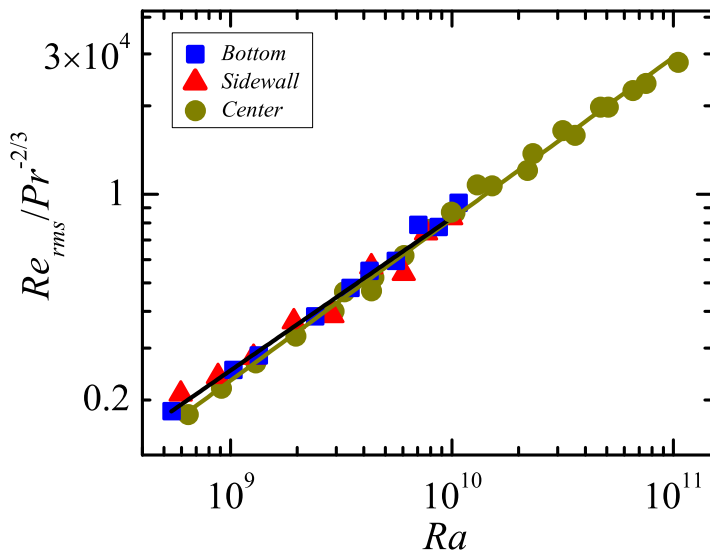
FIG. 3. The Reynolds number Re_{rms} measured in different regions as a function of the Ra number. The data are calculated from the rms value of the Lagrangian velocity and compensated by a $Pr^{-2/3}$ dependence according to the model proposed by Grossmann and Lohse [27–30].

that the Lagrangian velocity in these regions have been affected by the inhomogeneity of the mean flow, as pointed out in the study by Liot *et al.* [57]. To our knowledge, their study was the only experimental work focusing on the Lagrangian velocity statistics in turbulent convection before. Their measurement was made in the central region of an octagonal convection cell with Ra = 2.0×10^{10} (close to our highest Ra) and Pr = 4.4, but the measurement volume was so large that both the bulk flow and part of the large-scale mean flow were captured simultaneously in their study. They found that the pdf of the vertical velocity follows the Gaussian distribution, which is consistent with our present results; however, the two horizontal components are found to be highly non-Gaussian, which is attributed to the inhomogeneity and unsteadiness of the mean flow. On the other hand, Eulerian measurements revealed Gaussian-like pdf's for all the velocity components in the central region, but the behaviors in the bottom and sidewall regions were found to be deviated from the Gaussian form and become asymmetric [65,66]. The results obtained in different studies are not fully consistent, plausibly due to the fact that the experiments were conducted in different sizes of measurement volumes and even in convection cells with different geometries; thus different flow dynamics might be involved. Further dedicated experiments are needed to fully resolve this issue.

Based on the rms values of the Lagrangian velocity, we can further calculate the Lagrangian Reynolds number in different regions as shown in Fig. 3. The data are compensated by a $Pr^{-2/3}$ dependence according to the model proposed by Grossmann and Lohse (GL model) [27–30]. It is seen that the data obtained in the bottom and sidewall regions are overall undistinguished from each other, but they are both slightly larger than the results measured in the central region for the low Ra range. This marginal difference in the magnitude of Re_{rms} between the plume-abundant regions and the center region leads to a visible difference in the Ra-dependent scaling exponent. To be specific, if a power-law fitting is attempted to the data in different regions, we obtain $Re_{rms} = 0.026 \, Ra^{0.55 \pm 0.01} Pr^{-2/3}$ for the center region and $Re_{rms} = 0.053 \, Ra^{0.52 \pm 0.02} Pr^{-2/3}$ for the plume-abundant regions. These scaling exponents are close to the values obtained in previous studies (varying from 0.4 to 0.5; see [1] for a review and also a recent study on this issue [67]). We do not have a clear explanation as to why the scaling exponents for these regions are larger than the free-fall-type value of 0.5, but observations of Re (Ra) scaling steeper than 0.5 are not
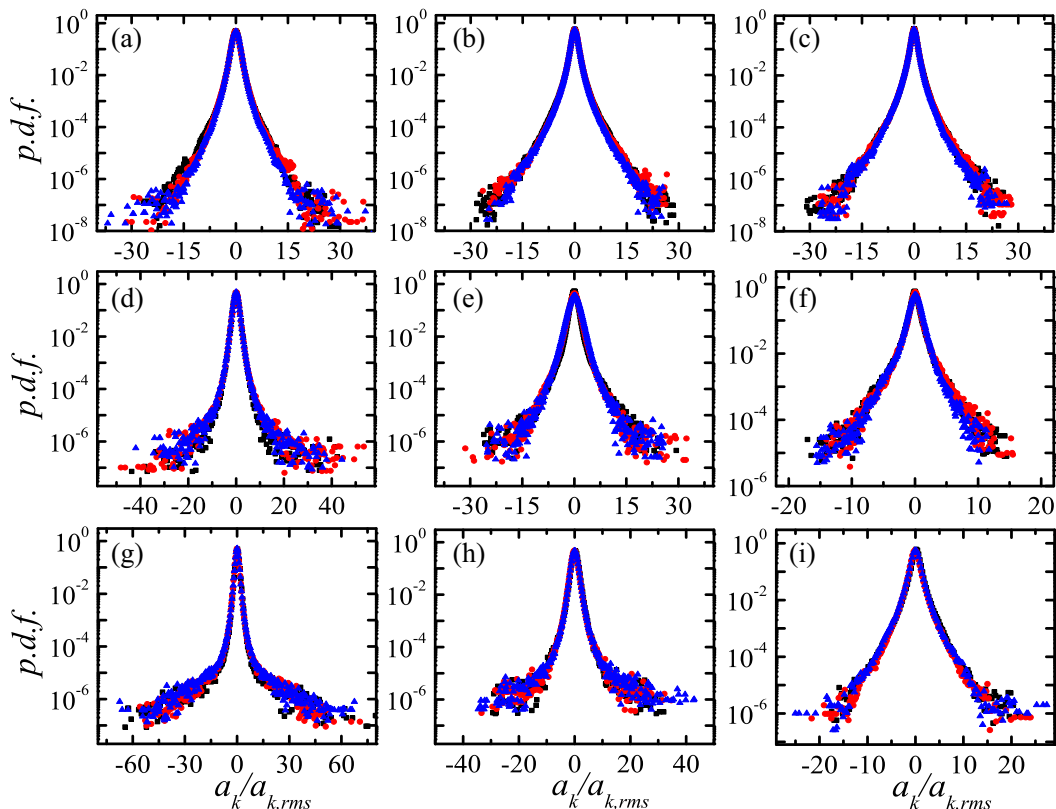
FIG. 4. The probability density functions (pdf's) of the three normalized acceleration components measured in different regions and at three representative Ra numbers, where $k = x, y$, and z. From top to bottom: Center region [(a), (b), (c)], sidewall region [(d), (e), (f)], and bottom region [(g), (h), (i)]. Left panel: Ra $\simeq 6 \times 10^8$; middle panel: Ra $\simeq 1.3 \times 10^9$; right panel: Ra $\simeq 1 \times 10^{10}$. For all the pdf's, red circle, blue triangle, and black square represent the x, y, and z components, respectively.

uncommon in previous studies [62,68–72]. In view of this, the physical origin of the abnormal Re (Ra) scaling deserves in-depth investigations in the future.

B. Acceleration statistics

Now we examine the Lagrangian acceleration statistics. Figure 4 shows the pdf's of the three acceleration components normalized by their own rms values at three representative Ra numbers, which are the smallest, medium, and highest Ra in the present study. We found that all the pdf's exhibit symmetric and stretched exponential shape as in other types of turbulent flows [52,73], indicating the strong intermittency of the flow. A somewhat unexpected finding here is that the vertical acceleration and the lateral ones almost fall on top of each other for all the cases, even in the plume-abundant regions. These results not only suggest that the acceleration properties in these regions are hardly affected by the mean flow, but also indicate that they are largely isotropic, at least in terms of first-order quantities. This behavior is in strong contrast to the Lagrangian velocity statistics as found in Fig. 2. It is noteworthy that the Lagrangian velocity and acceleration statistics do not necessarily manifest the same flow dynamics, which has been shown in the experimental study by Liot *et al.* [57]. In a previous numerical Lagrangian study of turbulent convection [74], it is found that the lateral accelerations have much flatter tails than the vertical one, which is ascribed
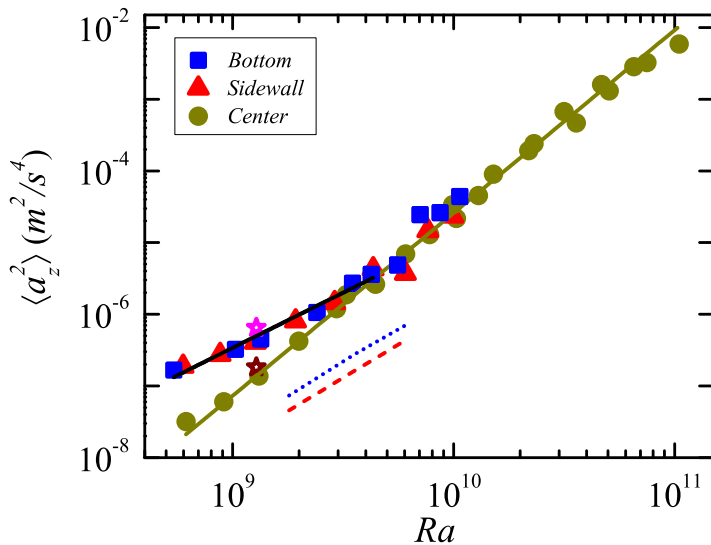
FIG. 5. The vertical acceleration variance as a function of Ra measured in different regions. The open stars are taken from another experimental study [58] for comparison, which were measured in the plume-abundant region (pink star) and the center region (magenta star) of a similar convection cell, respectively. Black solid line: $\langle a_z^2 \rangle \sim \mathrm{Ra}^{1.54 \pm 0.08}$ for the data measured in the plume-abundant regions with $\mathrm{Ra} \lesssim 4.3 \times 10^9$. Dark-yellow solid line: $\langle a_z^2 \rangle \sim \mathrm{Ra}^{2.55 \pm 0.11}$ for the data measured in the center region. The blue dotted line and red dash-dotted line are the results calculated from $\langle a^2 \rangle_{\mathrm{buoy}} = \langle (\alpha g \delta T)^2 \rangle$ for the bottom and sidewall regions, respectively. See text for the explanation.

to the vortical motions induced by thermal plumes. We do not observe this anisotropy here, which may be attributed to two factors: (i) in the numerical study, the statistics was taken over the whole volume, so many more plume-related events were captured; (ii) the different aspect ratios used in the two studies can result in different large-scale rolls and thus different spatial distribution of the plumes [59].

Nevertheless, we do find appreciable differences in the acceleration pdf's measured in different regions: while the pdf's obtained in the center region are almost identical for different Ra, the tails of the pdf's in the plume-abundant regions evolve with Ra number and stretch much more heavily for the lower Ra cases. For example, as shown in Fig. 4, the tails of the pdf's measured in the bottom region reach as far as 60 standard deviations at $\mathrm{Ra} \simeq 6 \times 10^8$; as Ra increases to 1.3×10^9, the tails become relatively narrower and they eventually become similar with the results in the center region at $\mathrm{Ra} \simeq 1 \times 10^{10}$. A similar feature is observed in the pdf's obtained in the sidewall region, though the tail stretching is not as strong as those in the bottom region. As a higher probability of observing large values of acceleration is a manifestation of more thermal plumes passing through the measurement volume [59,74], the pdf's in the plume-abundant regions suggest that there could be a different Lagrangian dynamics induced by thermal plumes for the lower Ra cases.

To reveal this different Lagrangian dynamics quantitatively, we plot in Fig. 5 the acceleration variance as a function of Ra number. Since the pdf's of the three acceleration components are nearly the same, we just focus on the vertical component for ease of presentation. It is seen from Fig. 5 that, while the acceleration variance in the center region can be well described by a single power law $\langle a_z^2 \rangle \sim \mathrm{Ra}^{2.55}$, the data in the plume-abundant regions exhibit two distinct regimes separated by $\mathrm{Ra} \lesssim 4.3 \times 10^9$. To be specific, for the lower Ra regime, the acceleration variance in the plume-abundant regions has a larger magnitude than that in the center region. This is consistent with the finding in a previous experimental study [58]. As Ra number increases, their difference in magnitude becomes smaller, and the data obtained in different regions start to follow approximately the same

trend for Ra greater than 4.3×10^9. To quantify this transitional behavior, we performed a power-law fit to the data in the plume-abundant regions with Ra $\lesssim 4.3 \times 10^9$ and the scaling exponent turns out to be 1.54, which is in sharp contrast to the value of 2.55 obtained in the center region. The different power laws imply that the Lagrangian acceleration in the plume-abundant regions with lower Ra should be governed by a different mechanism.

We first check whether this difference could be attributed to the effects of buoyancy force, which would be a natural candidate in turbulent RB convection. To do this, we assume that the acceleration is entirely generated by the buoyancy force. According to Eq. (1), the acceleration variance averaged over the measurement volume can be expressed as $\langle a^2 \rangle_{\text{buoy}} = \langle (\alpha g \delta T)^2 \rangle$. Here, $\delta T = (T - \langle T \rangle)$ is the instantaneous temperature difference for a fluid parcel and it can be obtained from the rms value of temperature fluctuation measured in the same volume, i.e., $\sigma_T = \sqrt{\langle (\delta T)^2 \rangle}$, which we adopt from results measured in the bottom and sidewall regions under conditions similar to those in the present study [5,6]. The values of $\langle a^2 \rangle_{\text{buoy}}$ thus obtained are shown as the blue dotted line and the red dash-dotted line, respectively for the bottom and sidewall regions, in Fig. 5. It is clear that the estimated $\langle a^2 \rangle_{\text{buoy}}$ are much smaller in magnitude than, and different scaling-wise from, the directly measured values. This suggests that the turbulent flow in the plume-abundant regions is not directly driven by local buoyancy force, which is in agreement with the analysis of local force balance in a recent numerical simulation [75]. Since the viscous term in Eq. (1) is negligible in the regions outside boundary layers [54,76], the pressure gradient term becomes the remaining plausible candidate.

C. Kinetic energy dissipation rate

It is extremely difficult, if impossible, to measure the pressure field generally in turbulent flows. However, we can resort to some analytical relations to understand how acceleration could be balanced when pressure gradient is dominant. The most well-documented one is the Heisenberg-Yaglom (HY) relation $\langle a^2 \rangle = a_0 \langle \epsilon_u \rangle^{3/2} \nu^{-1/2}$, where a_0 is the acceleration Kolmogorov constant [60,61]. In a previous study [56], we have found that the vertical acceleration variance in the center region follows the description of HY relation, indicating that the turbulent flow in this region is governed by forces arising from turbulent background fluctuations rather than buoyancy force. Here, we would like to examine whether the HY relation also holds in the plume-abundant regions.

To check this, we need to obtain the kinetic energy dissipation rate in the plume-abundant regions first. This can be calculated from the exact relations for the second-order longitudinal and transverse Eulerian SFs: $S_2^L(r) = \langle \epsilon_u \rangle r^2 / 15\nu$ and $S_2^N(r) = 2\langle \epsilon_u \rangle r^2 / 15\nu$, which are valid for homogeneous and isotropic turbulence in the dissipative range. The acceleration pdf's shown in Fig. 4 suggest that the plume-abundant regions may be approximately considered as locally homogeneous and isotropic. This is confirmed by the plateaus and the collapse of compensated SFs in the range with $r \lesssim \eta$, as shown in the inset of Fig. 6. This local isotropy and homogeneity are reasonable as our Lagrangian statistics are obtained within sufficiently small scales. Note that the data scatters in the smallest scales (mostly the first three points) are likely caused by insufficient statistics, as the probability is pretty low to find velocity pairs with very small separation r. From the plateau height of the compensated SFs, we obtain in Fig. 6 the Ra dependence of the kinetic energy dissipation rate. The data are normalized by $\text{Pr}^{1.15}$ as suggested in our previous study [77], which has a negligible effect on the Ra-dependent scaling. It is seen that, notwithstanding the data scatter, the kinetic dissipation rate in the plume-abundant regions also exhibits a transitional behavior: for Ra $\lesssim 4.3 \times 10^9$, the data can be fitted by a power law as $\langle \epsilon_u \rangle \sim \text{Ra}^{1.34}$, whereas for higher Ra, the data begin to follow the power-law trend as found in the center region. According to Grossmann and Lohse [27–30], the kinetic energy dissipation rate should scale as $\text{Ra}^{1.25}$ when plume dynamics is dominant, and the power law $\langle \epsilon_u \rangle \sim \text{Ra}^{1.50}$ will take over when turbulent background fluctuations become significant. The measured $\langle \epsilon_u \rangle \sim \text{Ra}^{1.34}$ relation seems to suggest that the flow dynamics in the plume-abundant regions for lower Ra might be determined by both thermal plumes and turbulent background fluctuations.
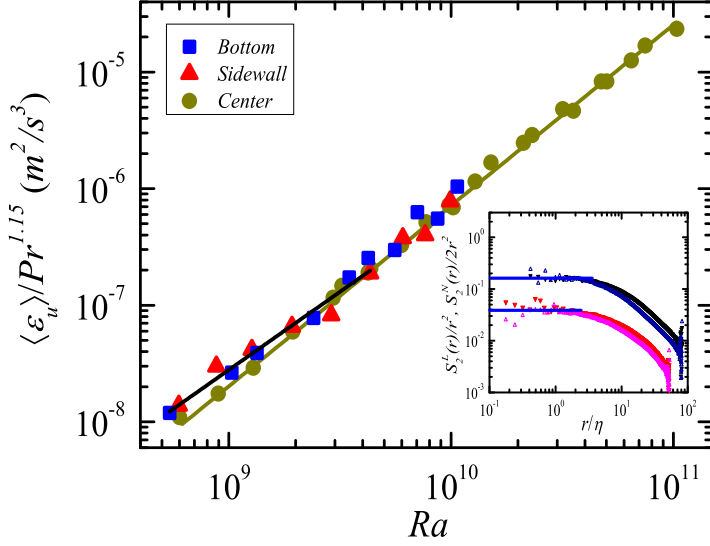
FIG. 6. The Ra dependence of the kinetic energy dissipation rates measured in different regions. The data are compensated by $Pr^{1.15}$ according to [77]. Black solid line: $\langle \epsilon_u \rangle \sim Ra^{1.34 \pm 0.07}$ for the data measured in the plume-abundant regions with Ra $\lesssim 4.3 \times 10^9$. Dark-yellow dashed line: $\langle \epsilon_u \rangle \sim Ra^{1.55 \pm 0.02}$ for the data measured in the cell center. Inset: Examples of the longitudinal (solid inverted triangle) and transverse (open upright triangle) second-order Eulerian structure functions compensated by the dissipative range scaling r^2 and $2r^2$, respectively. They are measured in the plume-abundant regions for Ra $\simeq 1.9 \times 10^9$ (lower data set) and Ra $\simeq 5.6 \times 10^9$ (upper data set). The blue horizontal lines indicate the plateau heights that are used to calculate the kinetic energy dissipation rates.

With the directly measured kinetic energy dissipation rate, we now check whether the HY relation holds in the plume-abundant regions. For Ra $\gtrsim 4.3 \times 10^9$, as with previous results obtained in the cell's central region, the HY relation predicts that $\langle a^2 \rangle \sim \langle \epsilon_u \rangle^{3/2} \sim Ra^{2.33 \pm 0.03}$, which is compatible with the directly measured result $\langle a_z^2 \rangle \sim Ra^{2.55 \pm 0.11}$. However, for Ra below 4.3×10^9, the Ra scaling predicted by the HY relation is 2.0 ± 0.1, which differs appreciably from the fitting exponent 1.54 ± 0.08 found in Fig. 5. To understand this discrepancy, we recall that the HY relation is derived for homogeneous and isotropic turbulence and assuming that the acceleration depends only on the kinetic energy dissipation and the viscosity. Considering the fact that thermal plumes in turbulent RB convection are both buoyant and thermal objects, the thermal dissipation rate should also be taken into account for the flow dynamics in the plume-abundant regions. In analogy to the different assumptions made respectively for the Kolmogorov and BO theories [40–42], we consider the scenario that the thermal dissipation rate ϵ_θ takes over the role of the kinetic energy dissipation rate; i.e., the flow dynamics is entirely dominated by thermal plumes. In this case, dimensional analysis leads to a relation analogous to the HY equation: $\langle a^2 \rangle = a_\theta (\alpha^2 g^2 \langle \epsilon_\theta \rangle)^{3/4} \kappa^{1/4}$, where a_θ is a new acceleration constant. For the Ra dependence of thermal dissipation rate, it has been found to be $\langle \epsilon_\theta \rangle \sim Ra^{1.67 \pm 0.03}$ for all the regions outside the boundary layers [50,78]. By substituting this result into the modified HY relation, we obtain $\langle a^2 \rangle \sim \langle \epsilon_\theta \rangle^{3/4} \sim Ra^{1.25 \pm 0.02}$, which still differs obviously from the experimental finding $\langle a_z^2 \rangle \sim Ra^{1.54 \pm 0.08}$. Notice that the measured exponent 1.54 is somehow in between the two predicted exponents (i.e., 2.0 and 1.25); it is natural to argue that the acceleration depends on both the thermal dissipation and the kinetic energy dissipation. Then similar dimensional analysis leads to another form of HY relation: $\langle a^2 \rangle \sim \langle \epsilon_\theta \rangle^{3/8} \langle \epsilon_u \rangle^{3/4} \sim Ra^{1.63 \pm 0.05}$. The predicted exponent 1.63 is much closer to the measured value of 1.54 if the experimental uncertainty is taken into account, suggesting that indeed both the thermal and kinetic dissipations may play a role in this Ra range. In other words, the scaling exponent is determined by the relative
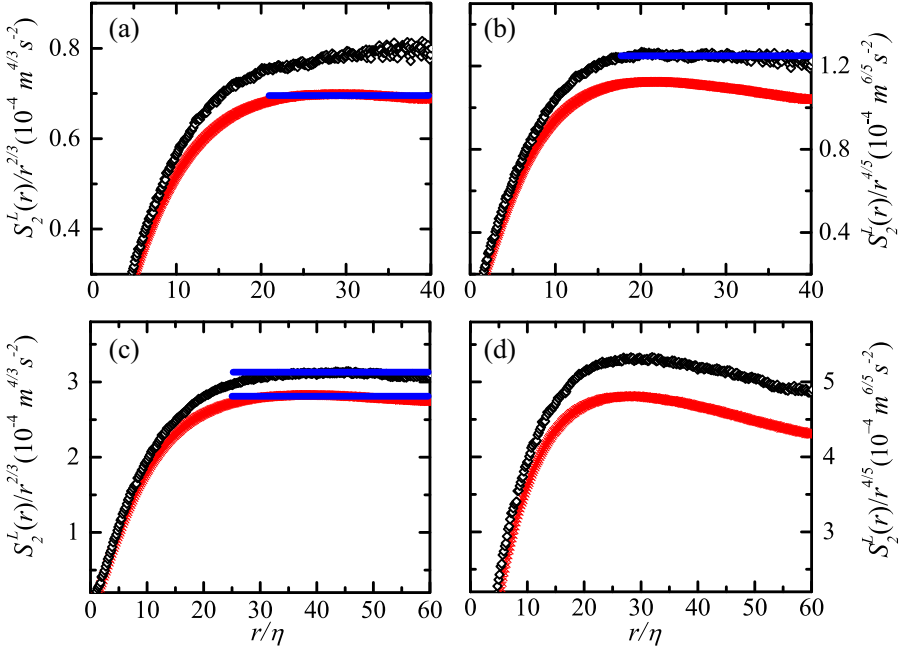
FIG. 7. The compensated second-order longitudinal Eulerian structure functions measured in the plume-abundant region (black square) and the center region (red cross). Left panel: Compensated by $r^{2/3}$; right panel: compensated by $r^{4/5}$. Top panel: Ra $\simeq 1.9 \times 10^9$; bottom panel: Ra $\simeq 7.0 \times 10^9$. The blue horizontal lines are used to guide the eye.

contributions from thermal plumes and turbulent background fluctuations, which is consistent with the Ra-dependent behavior of the kinetic energy dissipation rate aforementioned. In this context, the scaling exponents obtained here are effective values in the corresponding Ra ranges. This is in line with the central spirit of the prevalent models for turbulent convection proposed by Grossmann and Lohse [27–30].

The mixed dynamics picture reminds us of a previous study of Eulerian SFs in turbulent thermal convection under similar conditions [45]. By arguing that the energy cascade in the plume-abundant region is a result of the co-action of buoyancy and inertial forces, the authors of that study derived scaling exponents $\zeta_n = 2n/5$ for the Eulerian SFs $S_n(r)$ in the inertial range. Since Eulerian and Lagrangian frameworks are just two complementary approaches to describe fluid motions, the second-order Eulerian SF $S_2(r)$ constructed from the present Lagrangian data in the plume-abundant regions should follow the 4/5 scaling for the lower Ra cases. Indeed, as shown in Fig. 7, a clear plateau is observed when $S_2(r)$ measured in the plume-abundant regions at Ra $\simeq 1.9 \times 10^9$ is compensated by $r^{4/5}$; however, as Ra becomes larger than the transitional value of 4.3×10^9, a compensation with $r^{2/3}$ is preferred. On the other hand, for the center region, both data at lower and higher Ra cases are consistent with the classical Kolmogorov scaling for homogeneous and isotropic turbulence. Therefore, these Eulerian results are fully consistent with the Lagrangian acceleration and energy dissipation rate, and thus support the mixed dynamics scenario discussed above. Mixed dynamics in terms of local balance of a somewhat different nature has also been observed in a recent study [79]. In that case, different local force balances lead to different functional forms of temperature fluctuation profiles in different regions (plume eruption versus wind shearing) of the convection cell.

IV. CONCLUSION

In summary, we have made an experimental study of Lagrangian velocity and acceleration in the plume-abundant regions of turbulent RB convection. It is found that the pdf's of the three velocity components collapse with each other and follow Gaussian distribution for all the regions in the high Ra range, but they behave differently and deviate from the Gaussian function for lower Ra numbers. The Reynolds number Re_{rms} based on the rms velocity has a Rayleigh number scaling with exponent 0.52 in the plume-abundant regions, close to the value of 0.55 obtained in the region where plumes pass through much less frequently. By comparing with the data obtained in different regions of the convection cell, we found a different flow dynamics induced by thermal plumes, as manifested by the changes in the stretched tails of the acceleration pdf's, the Ra dependence of the acceleration variance, and also the kinetic energy dissipation rate. Through a detailed examination of the possible balances between acceleration and other small-scale properties, our results show that the acceleration in the plume-abundant regions is balanced with a combination of thermal and kinetic energy dissipation rates, which suggests that the turbulent flow in these regions is governed by a mixed process with contributions from both thermal plumes and turbulent background fluctuations. This picture is supported by the scaling laws of the Eulerian second-order structure functions in the inertial range. Thus, our present Lagrangian study has shed light on the role of thermal plumes in driving flow in turbulent RB convection.

Finally, we discuss the physical origins of the mixed dynamics and the transitional behaviors at Ra $\simeq 4.3 \times 10^9$. First of all, it is important to point out that even in the plume-abundant regions, thermal plumes could not occupy the whole volume, and turbulent background fluctuations always exist. So it is not surprising to observe that flow properties measured in these regions are governed by a mixed dynamics from both plumes and turbulent background. Another more important fact is that the flow path of the large-scale circulation (LSC, or the organized motion of thermal plumes) continuously evolves with increasing Ra [64,80]. As a result of this evolution, the geometric structure of the LSC changes from an ellipse positioned diagonally across the convection cell to a more squarish shape [64]. This means that as Ra increases, the organized motion of thermal plumes becomes closer to the periphery of the convection cell. On the other hand, because the measurement volumes in the present study were spatially fixed with their edges being ∼1.5 cm away from the bottom plate and the sidewall, thermal plumes will eventually move out of the measurement regions for higher Ra cases. Indeed, based on the flow path of the LSC given in [64], most of the thermal plumes have been moved out of the measurement regions at Ra $\simeq 4.3 \times 10^9$ in the present study. Consequently, the relative contributions of thermal plumes and turbulent background also change with increasing Ra, and the turbulent background becomes dominant when Ra is larger than 4.3×10^9. Therefore, the transitional behaviors observed in the present study can be understood as a result of the evolution in the flow path of the LSC or changes in flow structure morphology. It is noteworthy that, due to this morphological change in flow structure, a transition between two types of Re (Ra) scaling based on Eulerian measurements has also been observed in some previous studies [67,81]. In this context, one should study the flow dynamics pertaining to thermal plumes via conditional statistics as suggested in Ref. [49]. This requires spatial information of both temperature and velocity being measured simultaneously, which remains technically inaccessible for the requirements of the present study in terms of resolution and accuracy.

---

[1] G. Ahlers, S. Grossmann, and D. Lohse, Heat transfer and large scale dynamics in turbulent Rayleigh-Bénard convection, Rev. Mod. Phys. **81**, 503 (2009).

[2] D. Lohse and K.-Q. Xia, Small-scale properties of turbulent Rayleigh-Bénard convection, Annu. Rev. Fluid Mech. **42**, 335 (2010).

[3] F. Chillà and J. Schumacher, New perspectives in turbulent Rayleigh-Bénard convection, Eur. Phys. J. E **35**, 58 (2012).

[4] K.-Q. Xia, Current trends and future directions in turbulent thermal convection, Theor. Appl. Mech. Lett. **3**, 052001 (2013).

[5] X.-D. Shang, X.-L. Qiu, P. Tong, and K.-Q. Xia, Measured Local Heat Transport in Turbulent Rayleigh-Bénard Convection, Phys. Rev. Lett. **90**, 074501 (2003).

[6] X.-D. Shang, X.-L. Qiu, P. Tong, and K.-Q. Xia, Measurements of the local convective heat flux in turbulent Rayleigh-Bénard convection, Phys. Rev. E **70**, 026308 (2004).

[7] Y. Gasteuil, W. L. Shew, M. Gibert, F. Chillà, B. Castaing, and J.-F. Pinton, Lagrangian Temperature, Velocity, and Local Heat Flux Measurement in Rayleigh-Bénard Convection, Phys. Rev. Lett. **99**, 234302 (2007).

[8] R. Lakkaraju, R. J. A. M. Stevens, R. Verzicco, S. Grossmann, A. Prosperetti, C. Sun, and D. Lohse, Spatial distribution of heat flux and fluctuations in turbulent Rayleigh-Bénard convection, Phys. Rev. E **86**, 056315 (2012).

[9] S.-D. Huang, M. Kaczorowski, R. Ni, and K.-Q. Xia, Confinement-Induced Heat-Transport Enhancement in Turbulent Thermal Convection, Phys. Rev. Lett. **111**, 104501 (2013).

[10] K. L. Chong, S.-D. Huang, M. Kaczorowski, and K.-Q. Xia, Condensation of Coherent Structures in Turbulent Flows, Phys. Rev. Lett. **115**, 264503 (2015).

[11] S.-D. Huang and K.-Q. Xia, Effects of geometric confinement in quasi-2-D turbulent Rayleigh-Bénard convection, J. Fluid Mech. **794**, 639 (2016).

[12] K. L. Chong, Y. Yang, S. D. Huang, J.-Q. Zhong, R. J. A. M. Stevens, R. Verzicco, D. Lohse, and K.-Q. Xia, Confined Rayleigh-Bénard, Rotating Rayleigh-Bénard, and Double Diffusive Convection: A Unifying View on Turbulent Transport Enhancement through Coherent Structure Manipulation, Phys. Rev. Lett. **119**, 064501 (2017).

[13] Z. L. Lim, K. L. Chong, G.-Y. Ding, and K.-Q. Xia, Quasistatic magnetoconvection: Heat transport enhancement and boundary layer crossing, J. Fluid Mech. **870**, 519 (2019).

[14] S.-Q. Zhou and K.-Q. Xia, Plume Statistics in Thermal Turbulence: Mixing of an Active Scalar, Phys. Rev. Lett. **89**, 184502 (2002).

[15] S.-Q. Zhou, Y.-C. Xie, C. Sun, and K.-Q. Xia, Statistical characterization of thermal plumes in turbulent thermal convection, Phys. Rev. Fluids **1**, 054301 (2016).

[16] Q. Zhou, C. Sun, and K.-Q. Xia, Morphological Evolution of Thermal Plumes in Turbulent Rayleigh-Bénard Convection, Phys. Rev. Lett. **98**, 074501 (2007).

[17] Q. Zhou and K.-Q. Xia, Physical and geometrical properties of thermal plumes in turbulent Rayleigh-Bénard convection, New J. Phys. **12**, 075006 (2010).

[18] J. Bosbach, S. Weiss, and G. Ahlers, Plume Fragmentation by Bulk Interactions in Turbulent Rayleigh-Bénard Convection, Phys. Rev. Lett. **108**, 054501 (2012).

[19] E. S. C. Ching, H. Guo, X.-D. Shang, P. Tong, and K.-Q. Xia, Extraction of Plumes in Turbulent Thermal Convection, Phys. Rev. Lett. **93**, 124501 (2004).

[20] O. Shishkina and C. Wagner, Analysis of sheet-like thermal plumes in turbulent Rayleigh-Bénard convection, J. Fluid Mech. **599**, 383 (2008).

[21] E. P. van der Poel, R. Verzicco, S. Grossmann, and D. Lohse, Plume emission statistics in turbulent Rayleigh-Bénard convection, J. Fluid Mech. **772**, 5 (2015).

[22] L. P. Kadanoff, Turbulent heat flow: Structures and scaling, Phys. Today **54**(8), 34 (2001).

[23] H.-D. Xi, S. Lam, and K.-Q. Xia, From laminar plumes to organized flows: The onset of large-scale circulation in turbulent thermal convection, J. Fluid Mech. **503**, 47 (2004).

[24] D. Funfschilling and G. Ahlers, Plume Motion and Large-Scale Circulation in a Cylindrical Rayleigh-Bénard Cell, Phys. Rev. Lett. **92**, 194502 (2004).

[25] H.-D. Xi, S.-Q. Zhou, Q. Zhou, T.-S. Chan, and K.-Q. Xia, Origin of the Temperature Oscillation in Turbulent Thermal Convection, Phys. Rev. Lett. **102**, 044503 (2009).

[26] R. J. A. M. Stevens, H. J. H. Clercx, and D. Lohse, Effect of plumes on measuring the large scale circulation in turbulent Rayleigh-Bénard convection, Phys. Fluids **23**, 095110 (2011).

[27] S. Grossmann and D. Lohse, Scaling in thermal convection: A unifying theory, J. Fluid Mech. **407**, 27 (2000).

[28] S. Grossmann and D. Lohse, Thermal Convection for Large Prandtl Numbers, Phys. Rev. Lett. **86**, 3316 (2001).

[29] S. Grossmann and D. Lohse, Fluctuations in turbulent Rayleigh-Bénard convection: The role of plumes, Phys. Fluids **16**, 4462 (2004).

[30] R. J. A. M. Stevens, E. P. van der Poel, S. Grossmann, and D. Lohse, The unifying theory of scaling in thermal convection: The updated prefactors, J. Fluid Mech. **730**, 295 (2013).

[31] U. Burr, W. Kinzelbach, and A. Tsinober, Is the turbulent wind in convective flows driven by fluctuations? Phys. Fluids **15**, 2313 (2003).

[32] K.-Q. Xia, C. Sun, and S.-Q. Zhou, Particle image velocimetry measurement of the velocity field in turbulent thermal convection, Phys. Rev. E **68**, 066303 (2003).

[33] A. Liberzon, B. Lüthi, M. Guala, W. Kinzelbach, and A. Tsinober, Experimental study of the structure of flow regions with negative turbulent kinetic energy production in confined three-dimensional shear flows with and without buoyancy, Phys. Fluids **17**, 095110 (2005).

[34] S. B. Pope, *Turbulent Flows* (Cambridge University Press, Cambridge, 2000).

[35] F. F. Araujo, S. Grossmann, and D. Lohse, Wind Reversals in Turbulent Rayleigh-Bénard Convection, Phys. Rev. Lett. **95**, 084502 (2005).

[36] E. Brown and G. Ahlers, Large-Scale Circulation Model for Turbulent Rayleigh-Bénard Convection, Phys. Rev. Lett. **98**, 134501 (2007).

[37] M. Bukai, A. Eidelman, T. Elperin, N. Kleeorin, I. Rogachevskii, and I. Sapir-Katiraie, Effect of large-scale coherent structures on turbulent convection, Phys. Rev. E **79**, 066302 (2009).

[38] Q. Zhou and K.-Q. Xia, The mixing evolution and geometric properties of a passive scalar field in turbulent Rayleigh-Bénard convection, New J. Phys. **12**, 083029 (2010).

[39] K. R. Sreenivasan and R. A. Antonia, The phenomenology of small-scale turbulence, Annu. Rev. Fluid Mech. **29**, 435 (1997).

[40] A. N. Kolmogorov, The local structure of turbulence in incompressible viscous fluid for very large Reynolds numbers, Dokl. Acad. Nauk SSSR **30**, 301 (1941).

[41] J. R. Bolgiano, Turbulent spectra in a stably stratified atmosphere, J. Geophys. Res. **64**, 2226 (1959).

[42] A. Obukhov, Effect of Archimedean forces on the structure of the temperature field in a turbulent flow, Dokl. Acad. Nauk SSSR **125**, 1246 (1959).

[43] S. Ashkenazi and V. Steinberg, Spectra and Statistics of Velocity and Temperature Fluctuations in Turbulent Convection, Phys. Rev. Lett. **83**, 4760 (1999).

[44] E. Calzavarini, F. Toschi, and R. Tripiccione, Evidences of Bolgiano-Obhukhov scaling in three-dimensional Rayleigh-Bénard convection, Phys. Rev. E **66**, 016304 (2002).

[45] C. Sun, Q. Zhou, and K.-Q. Xia, Cascades of Velocity and Temperature Fluctuations in Buoyancy-Driven Thermal Turbulence, Phys. Rev. Lett. **97**, 144504 (2006).

[46] E. S. C. Ching, Scaling laws in the central region of confined turbulent thermal convection, Phys. Rev. E **75**, 056302 (2007).

[47] R. P. J. Kunnen, H. J. H. Clercx, B. J. Geurts, L. J. A. van Bokhoven, R. A. D. Akkermans, and R. Verzicco, Numerical and experimental investigation of structure-function scaling in turbulent Rayleigh-Bénard convection, Phys. Rev. E **77**, 016302 (2008).

[48] R. P. J. Kunnen and H. J. H. Clercx, Probing the energy cascade of convective turbulence, Phys. Rev. E **90**, 063018 (2014).

[49] E. S. C. Ching, Y.-K. Tsang, T. N. Fok, X. He, and P. Tong, Scaling behavior in turbulent Rayleigh-Bénard convection revealed by conditional structure functions, Phys. Rev. E **87**, 013005 (2013).

[50] M. Kaczorowski and K.-Q. Xia, Turbulent flow in the bulk of Rayleigh-Bénard convection: Small-scale properties in a cubic cell, J. Fluid Mech. **722**, 596 (2013).

[51] A. L. Porta, G. A. Voth, A. M. Crawford, J. Alexander, and E. Bodenschatz, Fluid particle accelerations in fully developed turbulence, Nature (London) **409**, 1017 (2001).

[52] G. A. Voth, L. A. Porta, A. M. Crawford, J. Alexander, and E. Bodenschatz, Measurement of particle accelerations in fully developed turbulence, J. Fluid Mech. **469**, 121 (2002).

[53] N. Mordant, A. M. Crawford, and E. Bodenschatz, Experimental Lagrangian acceleration probability density function measurement, Physica D (Amsterdam) **193**, 245 (2004).

[54] H. Xu, N. T. Ouellette, D. Vincenzi, and E. Bodenschatz, Acceleration Correlations and Pressure Structure Functions in High-Reynolds Number Turbulence, Phys. Rev. Lett. **99**, 204501 (2007).

[55] F. Toschi and E. Bodenschatz, Lagrangian properties of particles in turbulence, Annu. Rev. Fluid Mech. **41**, 375 (2009).

[56] R. Ni, S.-D. Huang, and K.-Q. Xia, Lagrangian acceleration measurements in convective thermal turbulence, J. Fluid Mech. **692**, 395 (2012).

[57] O. Liot, A. Gay, J. Salort, M. Bourgoin, and F. Chillà, Inhomogeneity and Lagrangian unsteadiness in turbulent thermal convection, Phys. Rev. Fluids **1**, 064406 (2016).

[58] H. Rajaei, P. Joshi, K. M. J. Alards, R. P. J. Kunnen, F. Toschi, and H. J. H. Clercx, Transitions in turbulent rotating convection: A Lagrangian perspective, Phys. Rev. E **93**, 043129 (2016).

[59] J.-T. Kim, S. Shen, S. L. DiMarco, Y. Jin, and L. P. Chamorro, Lagrangian acceleration in Rayleigh-Bénard convection at various aspect ratios, Phys. Rev. Fluids **3**, 113502 (2018).

[60] W. Heisenberg, Zur statistichen theorie der turbulenz, Z. Phys. **124**, 628 (1948).

[61] A. M. Yaglom, On the acceleration field in a turbulent flow, Dokl. Akad. Nauk SSSR **67**, 795 (1949).

[62] S. Lam, X.-D. Shang, S.-Q. Zhou, and K.-Q. Xia, Prandtl number dependence of the viscous boundary layer and the Reynolds numbers in Rayleigh-Bénard convection, Phys. Rev. E **65**, 066306 (2002).

[63] S.-L. Lui and K.-Q. Xia, Spatial structure of the thermal boundary layer in turbulent convection, Phys. Rev. E **57**, 5494 (1998).

[64] C. Sun and K.-Q. Xia, Scaling of the Reynolds number in turbulent thermal convection, Phys. Rev. E **72**, 067302 (2005).

[65] X.-L. Qiu and P. Tong, Large-scale velocity structures in turbulent thermal convection, Phys. Rev. E **64**, 036304 (2001).

[66] X.-L. Qiu, X.-D. Shang, P. Tong, and K.-Q. Xia, Velocity oscillations in turbulent Rayleigh-Bénard convection, Phys. Fluids **16**, 412 (2004).

[67] V. Musilová, T. Králík, M. La Mantia, M. Macek, P. Urban, and L. Skrbek, Reynolds number scaling in cryogenic turbulent Rayleigh-Bénard convection in a cylindrical aspect ratio one cell, J. Fluid Mech. **832**, 721 (2017).

[68] C. Sun, Y.-H. Cheung, and K.-Q. Xia, Experimental studies of the viscous boundary layer properties in turbulent Rayleigh-Bénard convection, J. Fluid Mech. **605**, 79 (2008).

[69] E. P. van der Poel, R. J. A. M. Stevens, and D. Lohse, Comparison between two- and three-dimensional Rayleigh-Bénard convection, J. Fluid Mech. **736**, 177 (2013).

[70] Y. Zhang, Q. Zhou, and C. Sun, Statistics of kinetic and thermal energy dissipation rates in two-dimensional turbulent Rayleigh–Bénard convection, J. Fluid Mech. **814**, 165 (2017).

[71] X. Chen, S.-D. Huang, K.-Q. Xia, and H.-D. Xi, Emergence of substructures inside the large-scale circulation induces transition in flow reversals in turbulent thermal convection, J. Fluid Mech. **877**, R1 (2019).

[72] X.-M. Li, J.-D. He, Y. Tian, P. Hao, and S.-D. Huang, Effects of Prandtl number in quasi-two-dimensional Rayleigh-Bénard convection, J. Fluid Mech. **915**, A60 (2021).

[73] L. Biferale, G. Boffetta, A. Celani, B. J. Devenish, A. Lanotte, and F. Toschi, Multifractal Statistics of Lagrangian Velocity and Acceleration in Turbulence, Phys. Rev. Lett. **93**, 064502 (2004).

[74] J. Schumacher, Lagrangian Dispersion and Heat Transport in Convective Turbulence, Phys. Rev. Lett. **100**, 134502 (2008).

[75] A. Pandey and M. K. Verma, Scaling of large-scale quantities in Rayleigh-Bénard convection, Phys. Fluids **28**, 095105 (2016).

[76] P. Vedula and P. K. Yeung, Similarity scaling of acceleration and pressure statistics in numerical simulations of isotropic turbulence, Phys. Fluids **11**, 1208 (1999).

[77] R. Ni, S.-D. Huang, and K.-Q. Xia, Local Energy Dissipation Rate Balances Local Heat Flux in the Center of Turbulent Thermal Convection, Phys. Rev. Lett. **107**, 174503 (2011).

[78] X. He, P. Tong, and K-Q. Xia, Measured Thermal Dissipation Field in Turbulent Rayleigh-Bénard Convection, Phys. Rev. Lett. **98**, 144501 (2007).

[79] Y.-H. He and K.-Q. Xia, Temperature Fluctuation Profiles in Turbulent Thermal Convection: A Logarithmic Dependence versus a Power-Law Dependence, Phys. Rev. Lett. **122**, 014503 (2019).

[80] J. J. Niemela and K. R. Sreenivasan, Rayleigh-number evolution of large-scale coherent motion in turbulent convection, Europhys. Lett. **62**, 829 (2003).

[81] E. Brown, D. Funfschilling, and G. Ahlers, Anomalous Reynolds-number scaling in turbulent Rayleigh-Bénard convection, J. Stat. Mech. (2007) P10005.